Generation and Evolution of Internal Waves in Luzon Strait

Ren-Chieh Lien
Applied Physics Laboratory
University of Washington
1013 NE 40th Street
Seattle, Washington 98105
Phone: (206) 685-1079 fax: (206) 543-6785 email: lien@apl.washington.edu

Frank Henyey
Applied Physics Laboratory
University of Washington
1013 NE 40th Street
Seattle, Washington 98105
Phone: (206) 543-4865 fax: (206) 543-6785 email: frank@apl.washington.edu

Award Number: N00014-09-1-0279

LONG-TERM GOALS

Our long-term scientific goals are to understand the dynamics and identify mechanisms of small-scale processes—i.e., internal tides, inertial waves, nonlinear internal waves (NLIWs), and turbulence mixing—in the ocean and thereby help develop improved parameterizations of mixing for ocean models. Mixing within the stratified ocean is a particular focus as the complex interplay of internal waves from a variety of sources and turbulence makes this a current locus of uncertainty. For this study, our focus is on generation, propagation, evolution, and dissipation of small-scale internal waves and internal tides as the Kuroshio and barotropic tides interact with the two prominent submarine ridges in Luzon Strait.

OBJECTIVES

The primary objectives of this observational program are to quantify 1) the generation of NLIWs and internal tides in the vicinity of Luzon Strait, 2) the energy flux of NLIWs and internal tides into the Pacific Ocean and South China Sea (SCS), 3) the effects of the Kuroshio on the generation and propagation of NLIWs and internal tides, 4) the seasonal variation of NLIWs and internal tides, and 5) to study other small-scale processes, e.g., hydraulics and instabilities along internal tidal beams and at the Kuroshio front.

APPROACH

Near-field

In the Luzon Strait (Fig. 1), observations were taken using the combined 600-m-long towed CTD chain (TOWCTD) equipped with 40 CTD sensors and the Doppler sonar on the R/V *Revelle*. These

Report Documentation Page

Form Approved
OMB No. 0704-0188

1. REPORT DATE	2. REPORT TYPE	3. DATES COVERED
30 SEP 2012		**00-00-2012 to 00-00-2012**

4. TITLE AND SUBTITLE	5a. CONTRACT NUMBER
Generation and Evolution of Internal Waves in Luzon Strait	5b. GRANT NUMBER
	5c. PROGRAM ELEMENT NUMBER
6. AUTHOR(S)	5d. PROJECT NUMBER
	5e. TASK NUMBER
	5f. WORK UNIT NUMBER
7. PERFORMING ORGANIZATION NAME(S) AND ADDRESS(ES) **University of Washington,Applied Physics Laboratory,1013 NE 40th St,Seattle,WA,98105**	8. PERFORMING ORGANIZATION REPORT NUMBER
9. SPONSORING/MONITORING AGENCY NAME(S) AND ADDRESS(ES)	10. SPONSOR/MONITOR'S ACRONYM(S)
	11. SPONSOR/MONITOR'S REPORT NUMBER(S)

12. DISTRIBUTION/AVAILABILITY STATEMENT
Approved for public release; distribution unlimited

13. SUPPLEMENTARY NOTES

14. ABSTRACT

15. SUBJECT TERMS

16. SECURITY CLASSIFICATION OF:			17. LIMITATION OF ABSTRACT	18. NUMBER OF PAGES	19a. NAME OF RESPONSIBLE PERSON
a. REPORT	b. ABSTRACT	c. THIS PAGE			
unclassified	**unclassified**	**unclassified**	**Same as Report (SAR)**	**11**	

instruments took high-frequency, $\Delta t < 1$ min, and high vertical resolution, $\Delta z = 5-20$ m, measurements of temperature, salinity, and density, and oceanic velocity from near the surface to ~600-m depth.

Far-field

Full water-column velocity and temperature observations were taken using one subsurface mooring with a near-bottom upward-looking 75-kHz ADCP and one surface mooring with three ADCPs, temperature loggers, and a series of CTD sensors at a sampling rate of $\Delta t = 1$ min, capable of measuring internal tides and nonlinear internal waves (NLIWs) on the continental slope east of Dongsha Island, ~200 n mi west of Luzon Strait (Fig. 1).

WORK COMPLETED

Near-field

From 25 July through 4 August 2011, we conducted an intensive survey in the Luzon Strait using a 600-m-long towed system (TOWCTD) equipped with 20–40 CTD sensors (Fig. 2). The TOWCTD is developed specifically for this experiment. It provides realtime CTD observation via inductive modem allowing us to identify the energetic small-scale processes in realtime. The primary scientific objectives of this cruise are 1) to measure nonlinear internal waves in Babuyan channel (Fig. 3), 2) to measure lee waves behind the sill west of Babuyan channel, 3) to quantify internal tide generation at the southern Luzon Strait, and 4) to measure internal tide evolution at the southern Luzon Strait. All CTD sensors take samples of temperature, salinity, and pressure at a 10-s interval.

Far-field

One surface-buoy mooring (TC1), one subsurface mooring (TC2), and two bottom pressure moorings (TC1-BPR and TC2-BPR) were deployed on the Dongsha slope from R/V *Ocean Researcher 1* of Taiwan on 27–31 May 2011. The surface and subsurface moorings were placed 6 km apart on the slope. Three ADCPs, fourteen CTD sensors, and three temperature loggers were equipped on the surface mooring (TC1). The subsurface mooring (TC2) was equipped with one 75-kHz ADCP, ten temperature sensors, and three CTD sensors. On 1–6 June 2011 the surface and subsurface moorings were recovered by the Taiwanese R/V *Ocean Researcher 2*. The subsurface mooring was redeployed with an upward-looking 75-kHz ADCP, without temperature or CTD sensors. It was recovered in August 2011 by the R/V *Ocean Researcher 3*.

RESULTS

Near-field

Satellite remote sensing images often capture NLIWs in the Babuyan channel, between the Luzon mainland and Fuga Island. These NLIWs are likely generated at a 200-m tall sill west of Babuyan channel. Two days of towed CTD measurements were made at Babuyan channel during the beginning of spring tide. We observed one sizeable nonlinear internal wave train about 10-km east of sill. The wave amplitude was about 10 m. This is the first in situ confirmation of nonlinear internal waves in the Babuyan channel (Fig. 2). The maximum current in the Babuyan channel flowed westward at about 1 m/s.

The evolution of a hydraulic jump between two Philippine islands, Fuga and Dalupiri islands, was observed by the TOWCTD system during the peak of the spring tide. Detailed temperature, salinity, and density variations associated with small-scale processes, likely a combination of hydraulic jumps, internal waves, and turbulence were observed. The hydraulic jump likely developed when the strong diurnal tidal flow reversed. The hydraulic jump has complex and three-dimensional signatures. Vertical overturnings were found between 100 and 300-m depth near 18.9°N. The maximum isopycnal displacement was ~100 m, and the maximum temperature change was ~4 °C along isopycnal surface. The hydraulic jump developed only during the spring tide. Because of their transient and complex three-dimensional structure, fast spatial sampling of temperature, salinity, density, and velocity measurements is needed to capture the evolution of the hydraulic jump (Fig. 3).

The towed CTD chain and the shipboard ADCP provided CTD and velocity observations in the upper 450 m near the generation site to the west of the eastern ridge in the southern Luzon Strait. Observed velocity and density are fitted to diurnal and semidiurnal frequency bands. The vertical profiles of eigenmodes are computed using shipboard CTD casts. Observed diurnal and semidiurnal velocity and density are projected to mode-1 vertical structure and the energy fluxes $F_x = <u'p'>$ and $F_y = <v'p'>$ are computed. Figure 4 shows the vertical profiles of diurnal and semidiurnal internal tidal energy fluxes averaged over 4 days of observations. Both diurnal and semidiurnal internal tidal energy fluxes are dominantly westward. Our observations in the upper 450 m capture ~65% of the energy flux, the remaining ~35% is inferred by the mode-1 projection. The depth integrated energy flux from the surface to 450-m is 10.4 kW/m for the diurnal tide and 11.7 kW/m for the semidiurnal tide. The full ocean depth integrated energy flux is 16 kW/m for the diurnal tide and 18 kW/m for semidiurnal tide (Fig. 4).

The estimates of the internal tidal energy flux are compared with those from the model prediction (with conditions appropriate for the time frame of our experiment) provided by Harper Simmons and with observations at mooring S9 (19.34° N, 121.03° E) taken by Matthew Alford. The diurnal tidal energy flux is 14 kW/m at mooring S9 and 16 kW/m at the TOWCTD site. The semidiurnal tidal energy flux is about 11 kW/m at mooring S9, and 18 kW/m at the TOWCTD site. The stronger flux at the TOWCTD site is consistent with the model prediction (Fig. 5). The model prediction suggests that the internal tides observed at S9 and TOWCTD site are from different generation sites.

Far-field

The far-field surface mooring provides full ocean depth observations of T, S, and velocity of internal tides and nonlinear internal waves. Nonlinear internal waves appear at a diurnal period (showing as spikes in temperature, salinity, and potential density). Measurements from a 600-kHz ADCP on the surface mooring and a 75-kHz ADCP on the subsurface mooring are combined to provide the full-ocean depth velocity profiles. Zonal velocity is stronger relative to the meridional velocity. The zonal velocity and vertical velocity also have a signal associated with nonlinear internal waves (Fig. 6).

Far-field mooring observations provide a direct estimate of internal tidal energy flux. The depth integrated diurnal internal tidal energy flux is 1.5 kW/m, much smaller than the 6.2 kW/m reported by *Chang et al.* [2006]. Their observations were made in April 2000 for 20 days. Our result of low diurnal energy flux is consistent with the model prediction by Harper Simmons. The model, in fact, predicts that the main internal diurnal tidal beam propagates south of our mooring site. The semidiurnal internal tidal energy flux is 4 kW/m, consistent with that reported by *Chang et al.* [2006], and with Simmons' model prediction. Dong Shang Ko's model also predicts an energy flux similar to Simmons'. The

diurnal tidal energy flux shows stronger variability than the semidiurnal tidal energy flux (Fig. 7) between 2000 and 2011, suggesting different north–south positions of the tidal beam at these two times.

Four large nonlinear internal waves were observed by the moorings. The wave propagation speed was computed using the arrival time between the subsurface mooring and surface mooring. The propagation speed was between 1.6 m/s and 1.9 m/s. The equilibrium depth of the maximum displacement varied in time from 60 m to 120 m. The wave amplitude computed from the isopycnal of maximum displacement varied from 100 m to 156 m. The wave amplitude increased from May 30 to June 3. The sum of available potential energy and kinetic energy increased from 298 MJ/m to 674 MJ/m. The maximum westward current increased from 1 to 2.15 m/s and the maximum vertical velocity increased from 0.2 to 0.72 m/s (Fig. 8).

The largest NLIW during our observation period was measured on June 3, 2011. There was a density inversion at the front end of the wave. It might indicate an overturning or inaccurate CTD measurements. We will investigate it further. At the rear end of wave, there were smaller density inversions, indicating mixing. The isopycnal displacement shows a typical mode-1 depression mode structure. The available potential energy was computed using both the linear approximation and the fully nonlinear form. These two estimates have similar values (Fig. 9). The zonal velocity of this largest NLIW has a possible trapped core formation where the current speed is greater than the propagation speed (Fig. 10, first panel; magenta closed contour). The vertical velocity contour shows strong downwelling in front of the wave, and strong upwelling after the wave. The vertical speed was as large as 0.72 m/s (Fig. 10, second panel). The kinetic energy was the strongest at the center of the wave. The kinetic and available potential energy have similar magnitudes (Fig. 10, third panel). The total kinetic energy was about 350 MJ/m, and the available potential energy was about 330 MJ/m (Fig. 10, bottom panel). We perform Dubreil–Jacotin–Long (DJL) model simulations of these waves with and without background shear. The wave speed is very well predicted. However, the DJL model does not predict the wave width and the energy very well, presumably because the observed NLIW was dissipative and unsteady on a shoaling slope, as reported in our *J. Phys. Oceanogr*. paper [Lien et al., 2012].

IMPACT/APPLICATION

Numerical models suggest strong internal tides are generated as barotropic tides interact with two prominent submarine ridges in the Luzon Strait. These internal tides are believed to be the sources of nonlinear internal waves often observed in the South China Sea. The strength of internal tides is modulated by the barotropic tidal forcing, the strength of the Kuroshio current, the background stratification, and the strength of the Kuroshio front. It is important to quantify the barotropic to baroclinic tidal energy conversion, dissipation within the Luzon Strait, the energy fluxes toward the South China Sea and Pacific Ocean, and the ultimate fate of the internal tidal energy.

RELATED PROJECTS

Energy Budget of Nonlinear Internal Waves Near Dongsha (N00014-05-1-0284) as a part of NLIWI DRI: In this project, we study the dynamics and quantify the energy budget of nonlinear internal waves (NLIWs) in the South China Sea using observations taken from two intensive shipboard experiments in 2005 and 2007 and a set of nearly one-year velocity-profile measurements taken in 2006–2007 from three bottom-mounted ADCPs across the continental slope east of Dongsha Plateau in

the South China Sea. Results of NLIWI DRI will help improve our understanding of the dynamics of NLIWs and will apply to the present project.

Process Study of Oceanic Responses to Typhoons Using Arrays of EM-APEX Floats and Moorings (N00014-08-1-0560) as a part of ITOP DRI: We study the dynamics of the oceanic response to and recovery from tropical cyclones in the western Pacific using long-term mooring observations and an array of EM-APEX floats. Pacific typhoons may cause cold pools on the continental shelf of the East China Sea. The cold pool dynamics are likely related to the Kuroshio and its intrusion as well as to shelf/slope oceanic processes.

PUBLICATIONS

Lien, R.-C., E.A. D'Asaro, F. Henyey, M.-H. Chang, T.-Y. Tang, Y.-J. Yang. 2012. Trapped core formation within a shoaling nonlinear internal wave. *J. Phys. Oceanogr.*, **42**, 511–525. doi: http://dx.doi.org/10.1175/2011JPO4578.1 . [refereed]

Farmer, D.M., M.H. Alford, R.-C. Lien, Y.J. Yang, M.-H. Chang, and Q. Li. 2011. From Luzon Strait to Dongsha Plateau: Stages in the life of an internal wave. *Oceanography* **24**(4):64–77, http://dx.doi.org/10.5670/oceanog.2011.95 . [refereed]

Chang, M.-H., R.-C. Lien, Y.-J. Yang, and T.-Y. Tang. 2011. Nonlinear internal wave properties estimated with moored ADCP measurements. *J. Atmos. Ocean. Technol.*, **28**, 802–815, doi: http://dx.doi.org/10.1175/2010JTECHO814.1 . [refereed]

Klymak, J.M., M.H. Alford, R. Pinkel, R.-C. Lien, Y.-J. Yang, and T.-Y. Tang. 2011. The breaking and xcattering of the internal tide on a continental Slope. *J. Phys. Oceanogr.*, **41**, 926–945, doi: http://dx.doi.org/10.1175/2010JPO4500.1 . [refereed]

Alford, M.H., R.-C. Lien, H. Simmons, J. Klymak, S. Ramp, Y.-J. Yang, D. Tang, and M.-H. Chang. 2010. Speed and evolution of nonlinear internal waves transiting the South China Sea. *J. Phys. Oceanogr.*, **40**, 1338–1355, doi: http://dx.doi.org/10.1175/2010JPO4388.1 . [refereed]

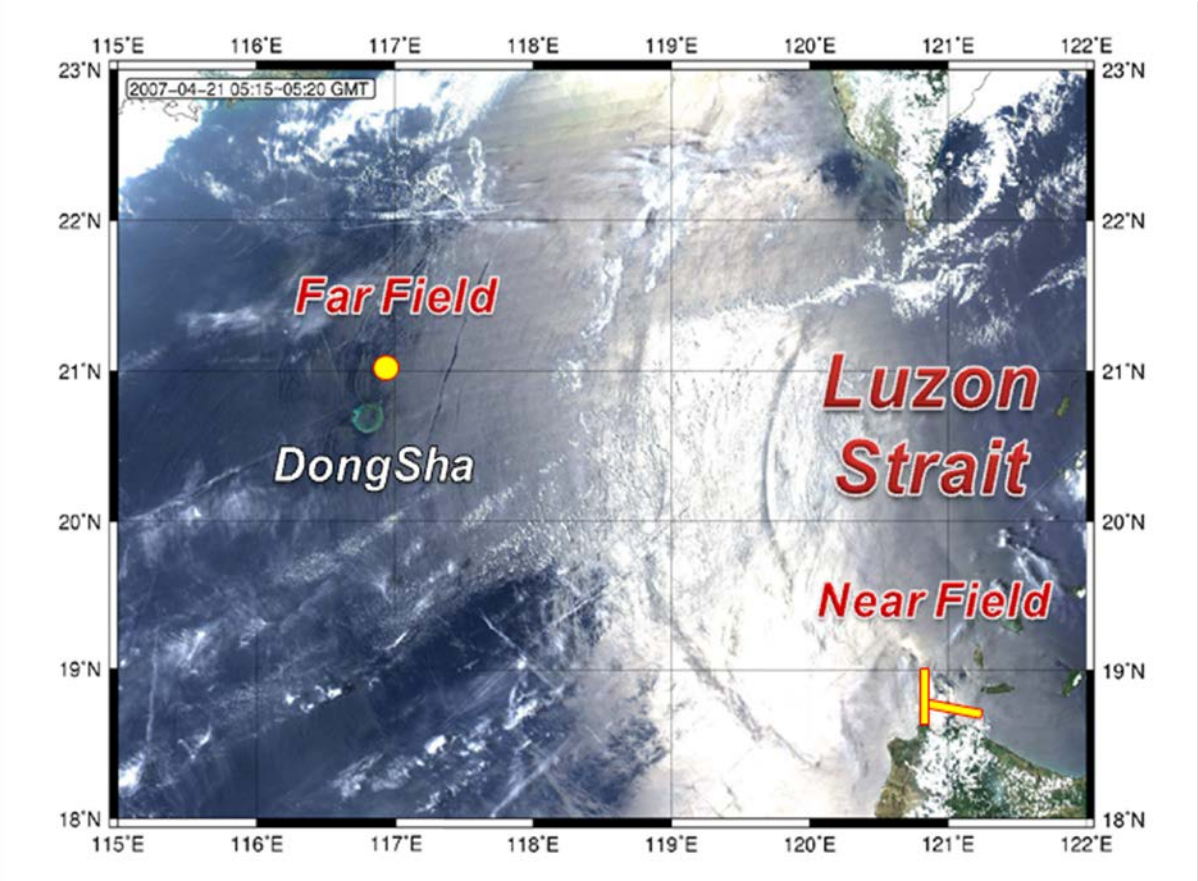

Figure 1. MODIS image taken in 2007 and the general area of near-field and far-field experiments. The near-field was performed using a towed CTD chain (TOWCTD) in July 25 – August 4, 2011 in the southern Luzon Strait (the two yellow boxes). The far-field was performed using a surface mooring and a subsurface mooring (yellow dot) in May 30 – July 3, 2011.

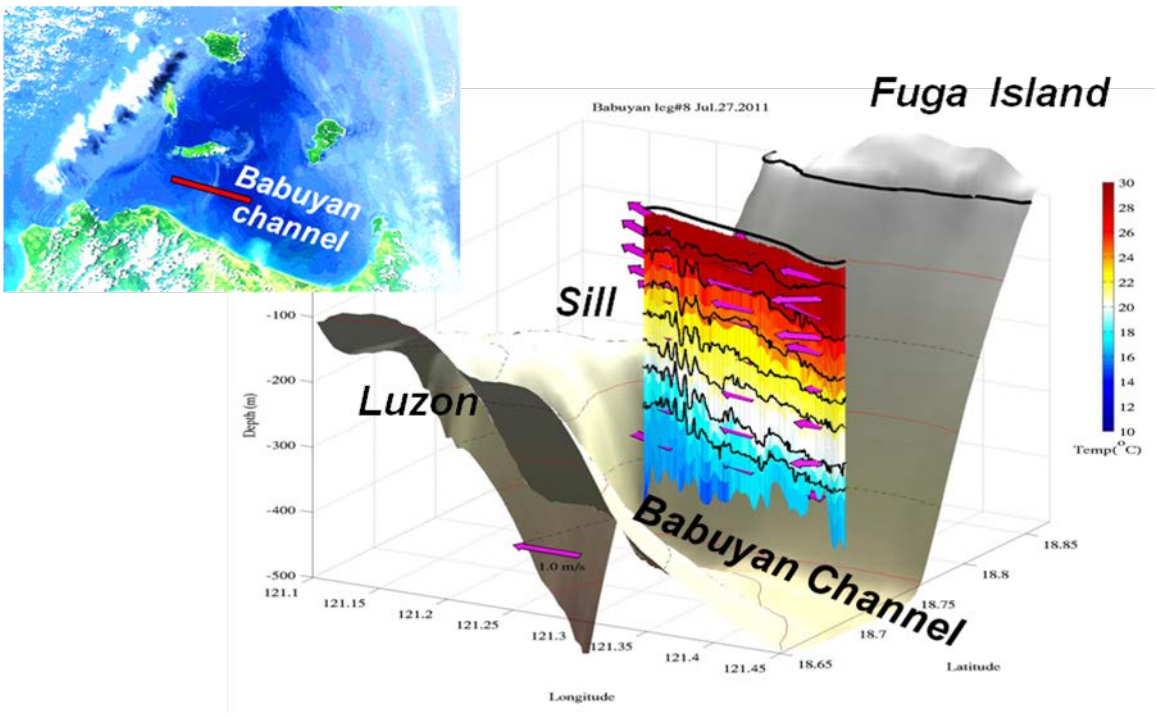

Figure 2. A small nonlinear internal wave train was observed at Babuyan channel (left panel) using the TOWCTD during the beginning of the spring tide. The red line shows the TOWCTD section. The temperature contours in the right panel are exaggerated by a factor of two to reveal the vertical structure of the wave train.

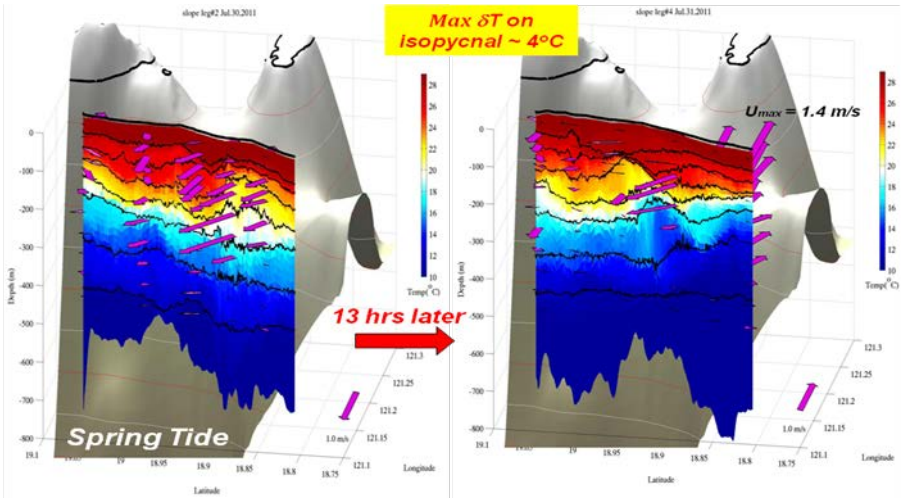

Figure 3. The evolution of a hydraulic jump between two Philippine islands, Fuga and Dalupiri islands, about 10 n mi north of Luzon during the peak of spring tide observed by the TOWCTD. Color shading represents the temperature contour. The black contour curves represent isopycnals. The magenta arrows show the current vectors. These two sections of observations were taken 13 hrs apart.

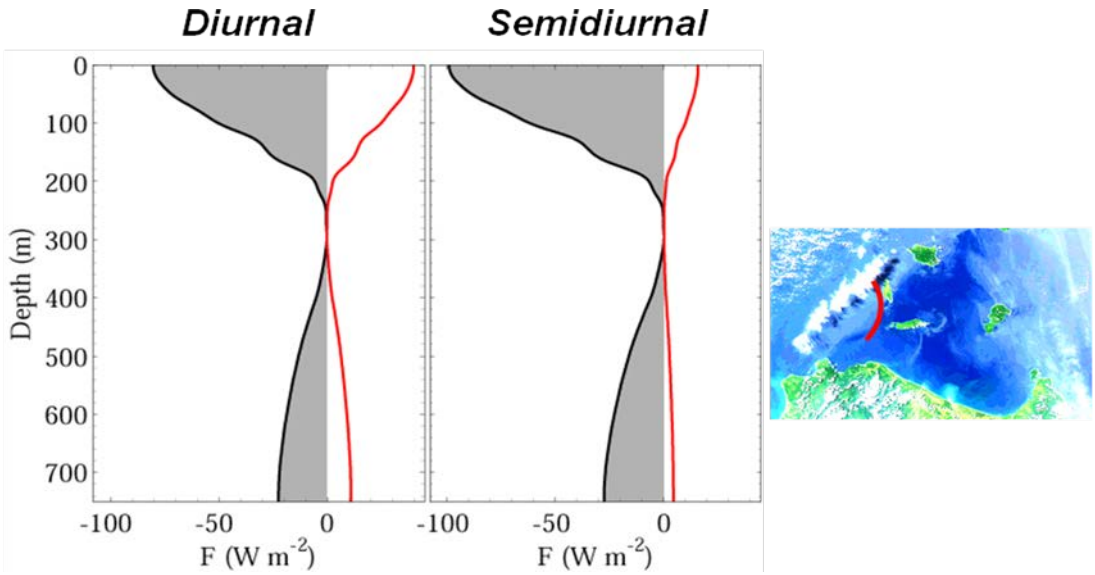

Figure 4. Diurnal and semidiurnal internal tidal energy flux near generation sites in southern Luzon Strait. Left, vertical profile of the zonal (gray shading) and the meridional (red curve) energy flux of the diurnal tide averaged along the TOWCTD section (red section in the right panel). Middle, vertical profile of the zonal (gray shading) and the meridional (red curve) energy flux of the semidiurnal tide averaged in the same section.

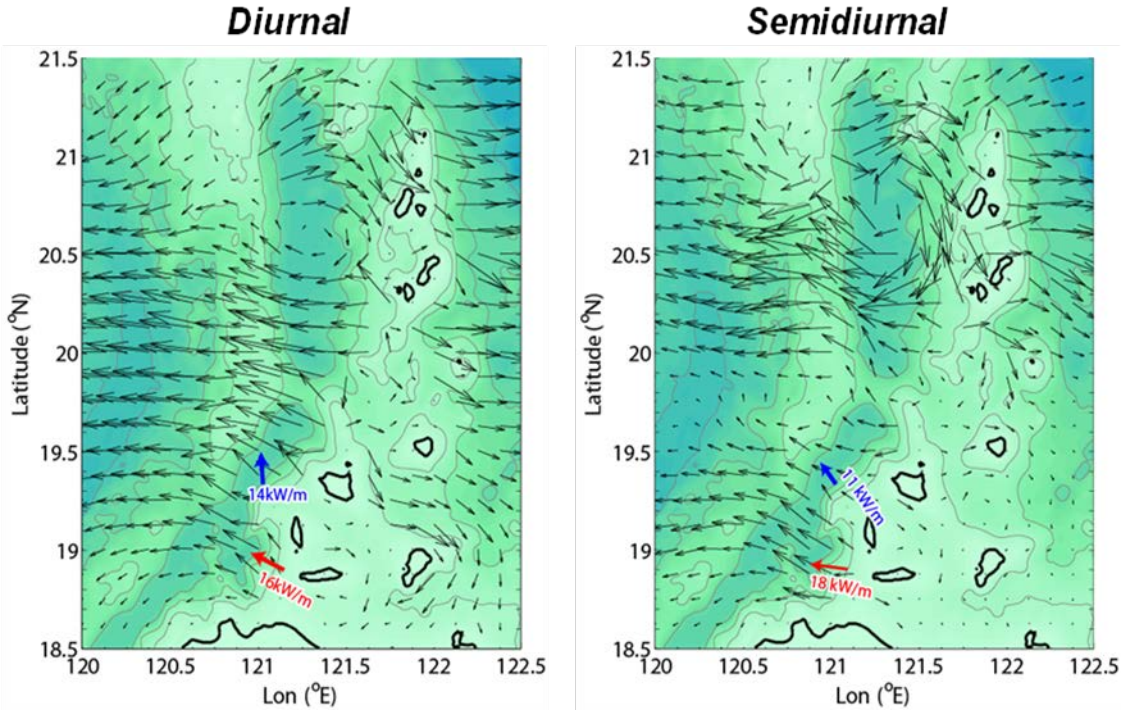

Figure 5. Comparison of the depth integrated diurnal and semidiurnal energy fluxes between model predictions (black arrows: Harper Simmons), S9 mooring observations (blue arrows: Matthew Alford), and TOWCTD observations (red arrows).

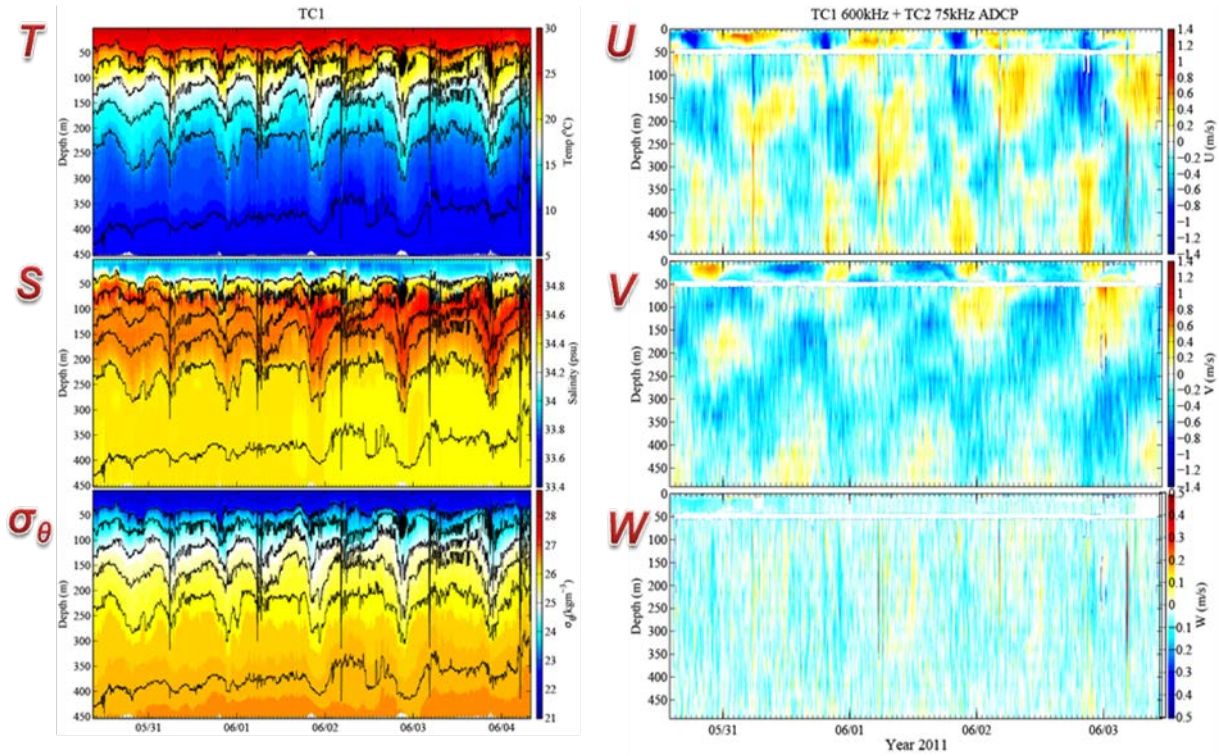

Figure 6. Left column, contour plots of temperature (top panel), salinity (middle panel), and density (bottom panel) taken from the far-field surface mooring (deployment May 30 – June 4, 2011). The black contour curves represent isopycnals. Right column, contours of zonal, meridional, and vertical velocity taken from the far-field moorings. These measurements provide full ocean depth observations of T, S, and velocity of internal tides and nonlinear internal waves.

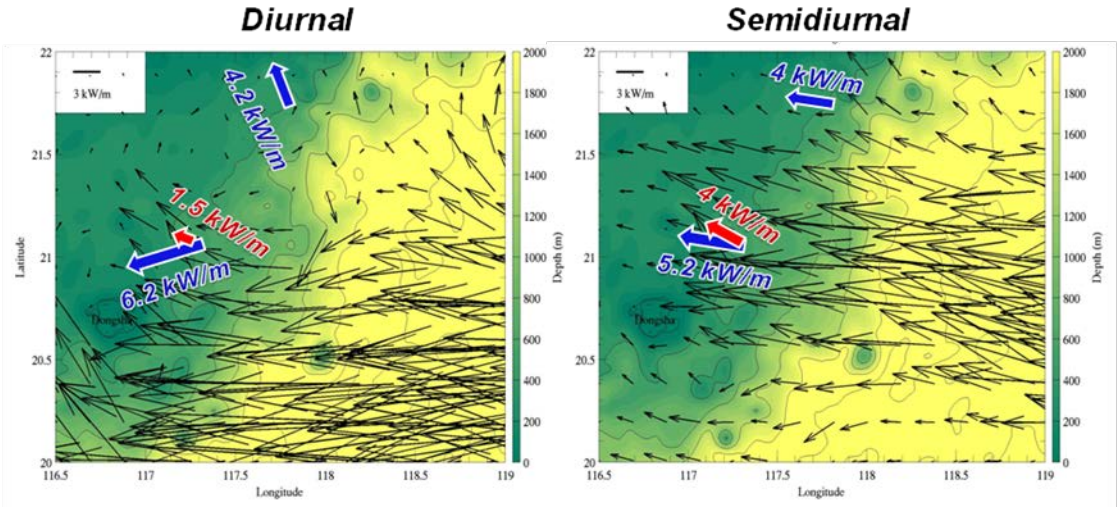

Figure 7. The diurnal and semidiurnal tidal energy flux from model predictions (black arrows: Harper Simmons), Chang's mooring observations in 2006 (blue arrows), and far-field mooring observations (red arrows).

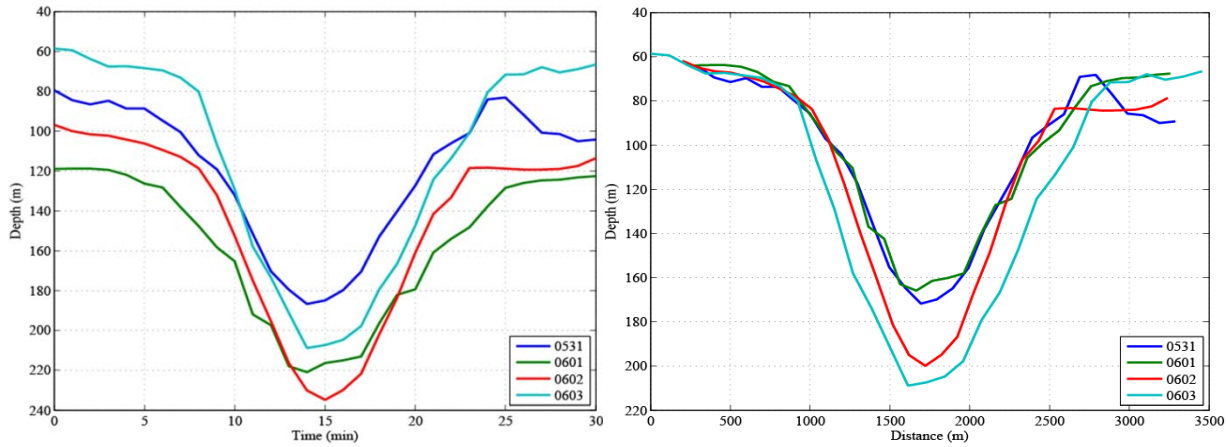

Figure 8. Left, isopycnal depths of the maximum displacement of NLIWs during May 31 and June 3. Right, isopycnal depths of the maximum displacement assuming a same equilibrium depth of 60 m.

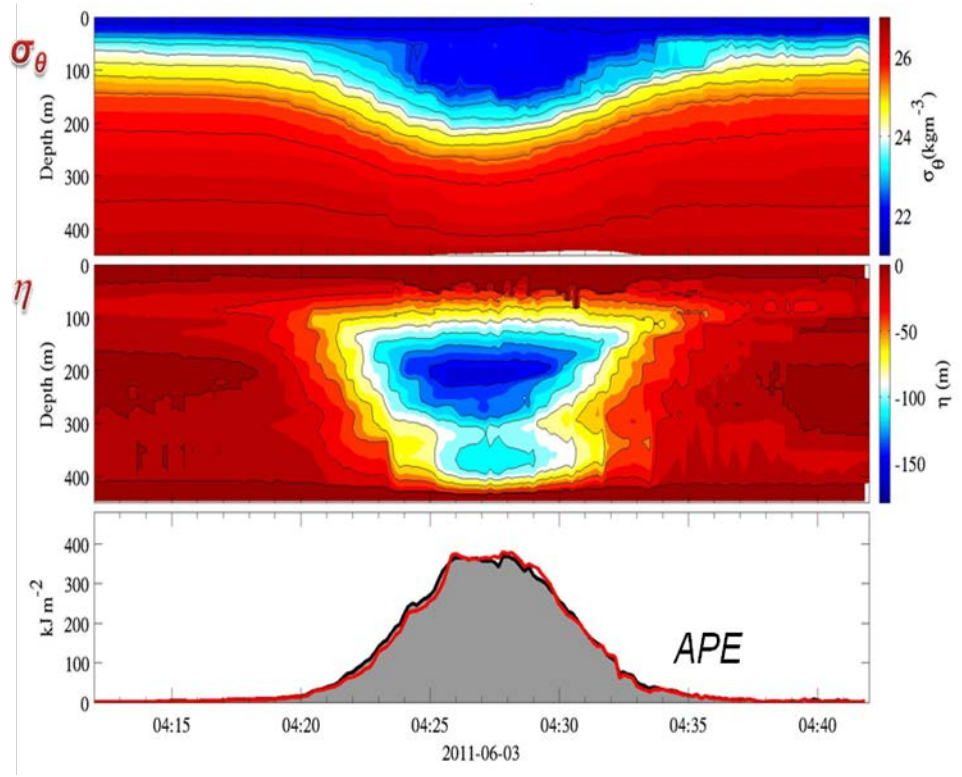

Figure 9. NLIW properties of June 3, 2011. Top, contour plot of density; middle, contour plot of vertical displacement; bottom, the depth integrated available potential energy calculated from two methods—fully nonlinear (black line) and linear approximation (red line).

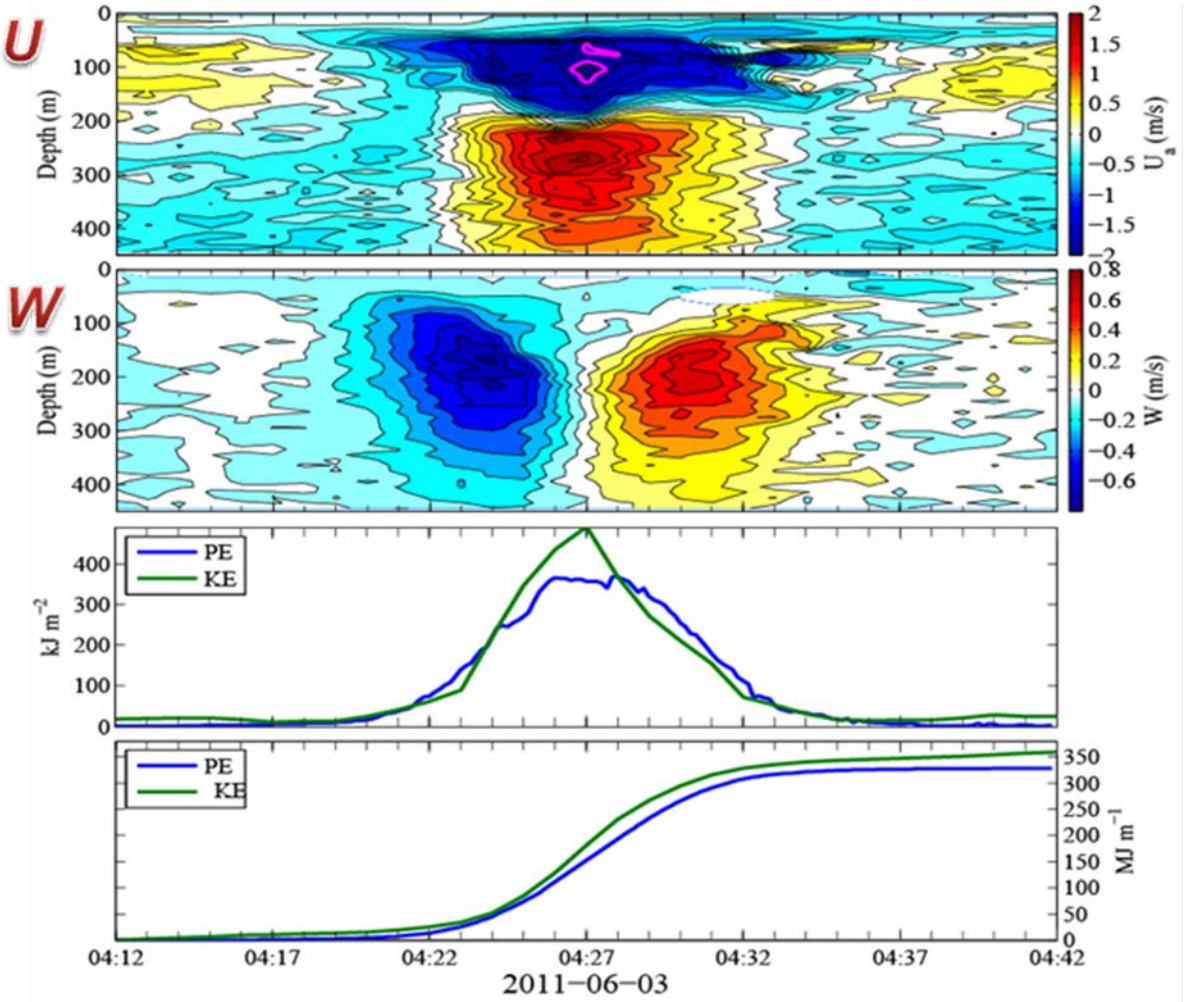

Figure 10. NLIW properties on June 3, 2011. Top, contour plot of the zonal velocity. The magenta closed contour line indicates the wave propagation speed. Second panel, contour plot of the vertical velocity. Third panel, depth integrated available potential energy (blue) and kinetic energy (green). Bottom, the accumulated available potential energy and kinetic energy.

REFERENCES

Chang, M.-H., R.-C. Lien, T.-Y. Tang, E.A. D'Asaro, and Y.-J. Yang. 2006. Energy flux of nonlinear internal waves in northern South China Sea, *Geophys. Res. Lett*., **33**, doi:10.1029/2005GL025196.

Lien, R.-C., E.A. D'Asaro, F. Henyey, M.-H. Chang, T.-Y. Tang, Y.-J. Yang. 2012. Trapped core formation within a shoaling nonlinear internal wave. *J. Phys. Oceanogr.*, **42**, 511–525. doi: http://dx.doi.org/10.1175/2011JPO4578.1 .